Research Square

Preprints are preliminary reports that have not undergone peer review.
They should not be considered conclusive, used to inform clinical practice,
or referenced by the media as validated information.

# Topology Optimization for Complex 3D Structures and Loading Conditions

**Jingchen Ye**
Xiamen University
**Qi Liu**
NORINCO Group Aviation Ammunition Institute
**Yu Feng**
Xiamen University
**Yanding Guo**
Jimei University
**Tieqiang Gang**
Xiamen University
**Lijie Chen**
chenlijie@xmu.edu.cn
Xiamen University

**Research Article**

**Keywords:** Topology optimization, Hybrid mesh, Volume-weighted density filtering, Time-varying load, Adjoint sensitivity analysis

**Posted Date:** November 11th, 2026

**DOI:** https://doi.org/10.21203/rs.3.rs-11419124/v1

**License:** This work is licensed under a Creative Commons Attribution 4.0 International License.
Read Full License

**Additional Declarations:** No competing interests reported.

# Topology Optimization for Complex 3D Structures and Loading Conditions

Jingchen Ye[a], Qi Liu[b], Yu Feng[a], Yanding Guo[c*], Tieqiang Gang[a], Lijie Chen[a*]

[a]School of Aerospace Engineering, Xiamen University, Xiamen 361102, China

[b]NORINCO Group Aviation Ammunition Institute, Harbin 150030, China

[c]College of Marine Equipment and Mechanical Engineering, Jimei University, Xiamen 361021, China.

**Abstract:**

Existing topology optimization methods are predominantly developed based on structured meshes and static loading assumptions, which result in insufficient geometric adaptability for complex three-dimensional structures and difficulties in accurately capturing transient dynamic responses encountered in practical engineering applications. To address these limitations, this study proposes a topology optimization method for complex three-dimensional structures based on hybrid-mesh discretization and transient dynamic response analysis. For mesh discretization, a hybrid mesh generation strategy combining tetrahedral and hexahedral elements is developed, with pentahedral pyramid elements employed as transition elements to ensure conformal connectivity and geometric compatibility between different mesh types, thereby enhancing the adaptability of the proposed method to complex geometries. In addition, a volume-weighted density filtering scheme is introduced to account for differences in element size during the smoothing of design variables, effectively suppressing the nonphysical influence of small-volume elements in transition regions on the density field. For topology optimization problems under time-varying loads, a transient topology optimization model is established based on transient adjoint sensitivity analysis, so as to make the optimization results of structural responses closer to the requirements of actual engineering conditions. Finally, several representative numerical examples are presented to demonstrate the effectiveness, numerical stability, and general applicability of the proposed method. The proposed approach provides an effective framework for high-accuracy topology optimization for complex 3D structures subjected to time-varying loads, offering both strong geometric adaptability and accurate transient dynamic analysis.

**Keywords:** Topology optimization; Hybrid mesh; Volume-weighted density filtering; Time-varying load; Adjoint sensitivity analysis

## 1. Introduction

In recent years, advances in high-performance computing and parallel finite element technologies have significantly enhanced the computational capability of large-scale topology optimization, thereby expanding its potential applications in aerospace lightweight structures and multifunctional structural design [1]. However, challenges remain in simultaneously improving computational efficiency, geometric

* Corresponding author: chenlijie@xmu.edu.cn (Lijie Chen); yandinggguo@jmu.edu.cn(Yanding Guo)

adaptability, and engineering applicability for complex three-dimensional structures [2,3].

Early studies on topology optimization mainly focused on structured meshes and compact numerical implementations. Sigmund [4] developed the well-known 99-line MATLAB code, which integrated the Solid Isotropic Material with Penalization (SIMP) method, finite element analysis, and the optimality criteria (OC) method into a unified framework, providing a fundamental platform for topology optimization research. Subsequently, Andreassen et al. [5] proposed a more compact 88-line MATLAB code that substantially improved computational efficiency and numerical stability through array preallocation, vectorized implementation, and density filtering. Talischi et al. [6] later developed the PolyTop framework based on unstructured polygonal finite element meshes, enabling two-dimensional topology optimization to accommodate complex design domains and arbitrary boundary geometries more flexibly. For three-dimensional topology optimization, Liu and Tovar [7] extended the density-based topology optimization approach to structured hexahedral meshes through the top3d program, providing an efficient and concise computational framework for three-dimensional structural optimization. Ferrari and Sigmund [8] further developed the top3D125 code by optimizing stiffness matrix assembly, density filtering, and design variable updating, thereby improving both computational efficiency and code compactness. Gao et al. [9,10] proposed an isogeometric topology optimization method based on density distribution functions and subsequently developed the IgaTop MATLAB program, promoting the integration of CAD-based geometric representation, finite element analysis, and topology optimization.

Although these methods have achieved significant progress in algorithmic efficiency, numerical implementation, and computational stability, they are primarily developed for regular design domains based on structured meshes. In contrast, engineering structures often exhibit irregular boundaries, complex curved surfaces, and rich local geometric features. The existing approaches still have limited geometric adaptability and it's difficult to balance accurate geometric representation with computational efficiency when applied to complex 3D structures.

Considering the applicability of topology optimization to irregular geometries, recently there are some studies on unstructured meshes, adaptive mesh refinement, and post-processing techniques for topology optimization results. Jia et al. [11] developed the FEniTop framework based on FEniCSx, which supports parallel computing, unstructured meshes, and large-scale three-dimensional examples, providing a new computational framework for efficient topology optimization in complex design domains. Li et al. [12] combined parallel computing, adaptive mesh refinement, and body-fitted tetrahedral meshing based on the level-set method to establish a topology optimization framework for full-scale three-dimensional structures, achieving high-resolution boundaries and high-quality optimized configurations. Xu et al. [13] proposed a voxel-to-tetrahedral mesh conversion method for density-based topology optimization results. By incorporating non-manifold repair, boundary smoothing, volume preservation, and feature-preserving simplification, the voxelized topology optimization results can be transformed into high-quality tetrahedral meshes suitable

for finite element analysis, design iteration, and manufacturing. These studies mainly focus on improving mesh generation efficiency, geometric representation quality, and manufacturability of optimization results, while systematic investigations of topology optimization based on hybrid meshes composed of different element types remain limited. In particular, significant differences in element size, volume, and neighborhood relationships between hexahedral and tetrahedral elements make conventional distance-based density filtering inadequate for accounting for variations in element volume during density updating, which may result in unstable optimization results. Therefore, developing a topology optimization framework capable of simultaneously considering geometric differences among hybrid mesh elements and transient dynamic characteristics remains an important research topic for complex three-dimensional structures.

On the other hand, engineering structures are frequently subjected to vibrations, impacts, and cyclic loads during service, resulting in pronounced transient dynamic responses. In this circumstance, it's necessary to promote topology optimization to adequately characterize the structural behavior under realistic operating conditions. Early work by Min et al. [14] established a topology optimization model with minimum dynamic compliance as the optimization objective, laying the foundation for topology optimization under dynamic loading. Subsequently, Choi and Park [15] proposed the equivalent static load (ESL) method, which transforms dynamic optimization problems into a sequence of static optimization problems by constructing equivalent static loads. Lee and Park [16] further extended the ESL method to nonlinear dynamic topology optimization. To improve the computational efficiency of transient dynamic topology optimization, Cao et al. [17] introduced an approximate dynamic response sensitivity analysis into the ESL framework. Guo et al. [18] further investigated topology optimization of transient thermoelastic structures subjected to time-dependent loads and demonstrated the importance of transient effects in multiphysics structural optimization. Guo's work established a thermoelastic topology optimization model based on the transient heat conduction equation and structural dynamic equilibrium equation, while employing adjoint sensitivity analysis to improve the computational efficiency of transient thermal stress responses and sensitivity evaluation. More recently, Saurabh et al. [19] developed a robust topology optimization framework considering uncertainties in the positions of transient dynamic loads, further reflecting the development trend of topology optimization under complex service conditions. Despite these advances, most studies are still conducted based on structured meshes, and a unified framework integrating hybrid-mesh discretization with transient dynamic topology optimization for complex three-dimensional structures has not yet been fully established.

Based on the above considerations, this study develops a hybrid-mesh topology optimization framework for complex three-dimensional structures subjected to time-varying loads. The proposed framework integrates hybrid-mesh finite element discretization, transient dynamic analysis, and topology optimization into a unified computational procedure. Representative numerical examples are designed to demonstrate the effectiveness and applicability of the proposed method.

## 2. Hybrid Mesh Generation Strategy

### 2.1 Applicability and Limitations of Single-Mesh Discretization Methods

The choice of finite element mesh has a direct influence on the geometric representation capability, computational accuracy, and efficiency of topology optimization. Hexahedral meshes have limited adaptability to complex boundaries and curved geometries, and are prone to geometric approximation errors and local mesh distortion. In contrast, tetrahedral meshes, although having superior automatic meshing capability and geometric adaptability, usually require more elements to achieve comparable accuracy, thereby increasing the degrees of freedom and computational cost. Moreover, their numerical performance is more sensitive to element quality and mesh density than that of hexahedral meshes [20].

To compare the displacement responses obtained using tetrahedral and hexahedral meshes in finite element analysis, a standard cantilever beam was selected as the benchmark example. As shown in Fig. 1, the design domain is a 50 mm × 25 mm × 5 mm rectangular beam, with the left end fully fixed and the end node of the right end subjected to a vertical static load to reproduce the loading condition. The displacement responses of the two mesh discretization models were then compared. Fig. 2 presents the displacement contour plots obtained under identical boundary and loading conditions.

As shown in Fig. 2, the results demonstrate that both mesh types accurately capture the overall displacement distribution of the structure, although slight differences exist in the predicted displacement magnitudes. The maximum displacement obtained by using the tetrahedral mesh is $4.256 \times 10^{-4}$mm, whereas that by using the hexahedral mesh is $4.916 \times 10^{-4}$mm. The absolute difference between the two predictions is $6.6 \times 10^{-5}$mm, corresponding to a relative difference of 15.51%. Under similar discretization conditions in this example, the tetrahedral mesh exhibits a significantly larger deviation in the predicted displacement than the hexahedral mesh. Considering the better numerical performance of the hexahedral mesh in the present benchmark problem, its solution is adopted as the reference for comparison.

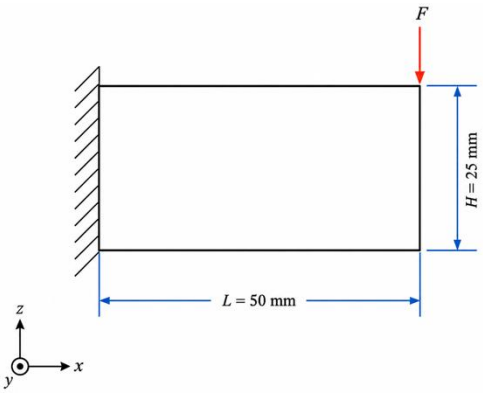
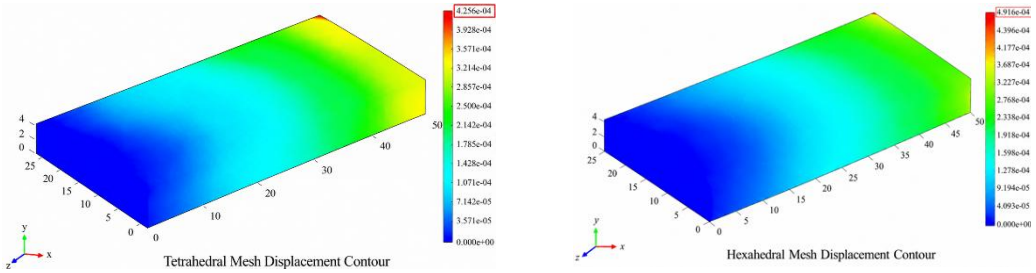



**Fig. 1.** Schematic of the cantilever beam.




(a) Displacement contour for cantilever beam with tetrahedral meshes

(b) Displacement contour for cantilever beam with hexahedral meshes

**Fig. 2.** Comparison of displacement contours for cantilever beam with tetrahedral and hexahedral meshes.

## 2.2 Hybrid Mesh Generation Strategy

Previous studies have demonstrated that employing tetrahedral meshes with strong geometric adaptability in complex geometric regions, while adopting structured meshes in regular regions, can effectively balance the discretization capability for complex boundaries and computational efficiency [21]. Therefore, a hybrid tetrahedral–hexahedral mesh generation strategy is proposed in the present topology optimization for complex 3D structures. According to the geometric characteristics and computational requirements of the structure, the design domain is discretized into different regions. Tetrahedral elements are employed in regions with complex boundaries, abrupt curvature variations, and local geometric details to enhance geometric adaptability. Meanwhile, hexahedral elements are adopted in regular structural regions to improve element quality and computational efficiency. Through the coordinated utilization of different element types, the proposed hybrid meshing strategy achieves a favorable balance among geometric adaptability, computational accuracy, and computational efficiency.

Because tetrahedral and hexahedral elements differ in both nodal configurations and face topologies, a direct conformal connection cannot be established between them. To ensure mesh conformity across adjacent regions, pyramid elements are introduced as transition elements to bridge triangular and quadrilateral faces. As illustrated in Fig. 3, the triangular side faces of a pyramid element are conformally connected to the neighboring tetrahedral elements, while its quadrilateral base is connected to the adjacent hexahedral element, thereby providing a continuous and compatible transition between different mesh regions.

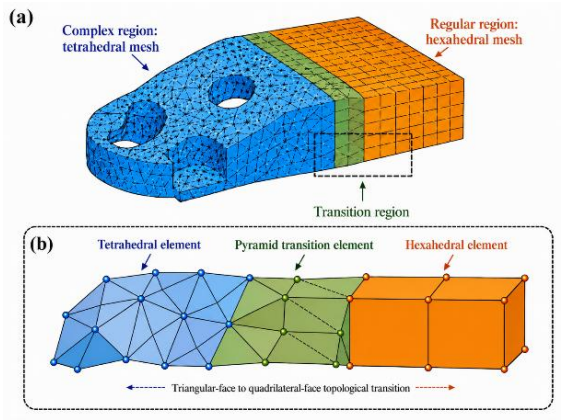



**Fig. 3.** Schematic illustration of the structure discretized with hybrid meshes.

## 2.3 Equivalent Decomposition of Pyramid Elements

Pyramid elements possess both triangular and quadrilateral geometric characteristics, making the construction of their shape functions, numerical integration schemes, and element matrices considerably more complicated than those of conventional tetrahedral and hexahedral elements. In addition, the nodal connectivity, face-topology compatibility, and element quality within the transition region have a direct influence on the accuracy and numerical stability of finite element analysis. To ensure a unified treatment of different element types in the hybrid-mesh finite element framework, each pyramid transition element is preprocessed prior to element matrix assembly. One pyramid element is equivalently decomposed into two tetrahedral sub-elements, allowing the evaluation of its stiffness matrix, mass matrix, and associated numerical integration to be consistently performed by using the tetrahedral element formulation [22,23], thereby improving the uniformity and computational feasibility of the implementation of the hybrid-mesh finite element program.

Consider a pyramid element with nodes numbered 1, 2, 3, 4 and 5, where nodes 1–4 constitute the quadrilateral base and node 5 represents the apex. The pyramid element is equivalently decomposed into two tetrahedral sub-elements, i.e., tetrahedral sub-element a: {1,2,3,5}, and tetrahedral sub-element b: {1,3,4,5}

Accordingly, the volume of the pyramid element $V_e$ is expressed as：

$$V_e = V_a + V_b,$$

Where $V_a$and $V_b$denote the volumes of tetrahedral sub-elements a and b, respectively. Then, the stiffness matrix $\mathbf{K}_e$ and mass matrix $\mathbf{M}_e$ of the pyramid element are assembled from the corresponding matrices of the two tetrahedral sub-elements as：

$$\begin{aligned} \mathbf{K}_e &= \mathbf{T}_a^{\mathrm{T}}\mathbf{K}_a\mathbf{T}_a + \mathbf{T}_b^{\mathrm{T}}\mathbf{K}_b\mathbf{T}_b, \\ \mathbf{M}_e &= \mathbf{T}_a^{\mathrm{T}}\mathbf{M}_a\mathbf{T}_a + \mathbf{T}_b^{\mathrm{T}}\mathbf{M}_b\mathbf{T}_b. \end{aligned} \tag{1}$$

where $\mathbf{K}_a$ and $\mathbf{K}_b$ are the stiffness matrices of tetrahedral sub-elements a and b, respectively; $\mathbf{M}_a$and $\mathbf{M}_b$denote the corresponding mass matrices; $\mathbf{T}_a$and $\mathbf{T}_b$are the transformation matrices that map the local degrees of freedom of the tetrahedral sub-elements to the global degrees of freedom of the pyramid element.

From the perspective of numerical implementation, the pyramid element is decomposed by introducing a diagonal on its quadrilateral base, thereby generating two non-overlapping tetrahedral sub-elements that completely cover the original geometric domain. Since both sub-elements employ the same linear interpolation functions, displacement continuity is naturally preserved through the shared nodes. Furthermore, this decomposition enables the direct reuse of the existing computational procedures for tetrahedral-element stiffness and mass matrices, eliminating the need for constructing the complex shape functions and numerical integration schemes required for pyramid elements. Consequently, the proposed treatment simplifies the implementation of the hybrid-mesh finite element program while improving its computational robustness and numerical stability.

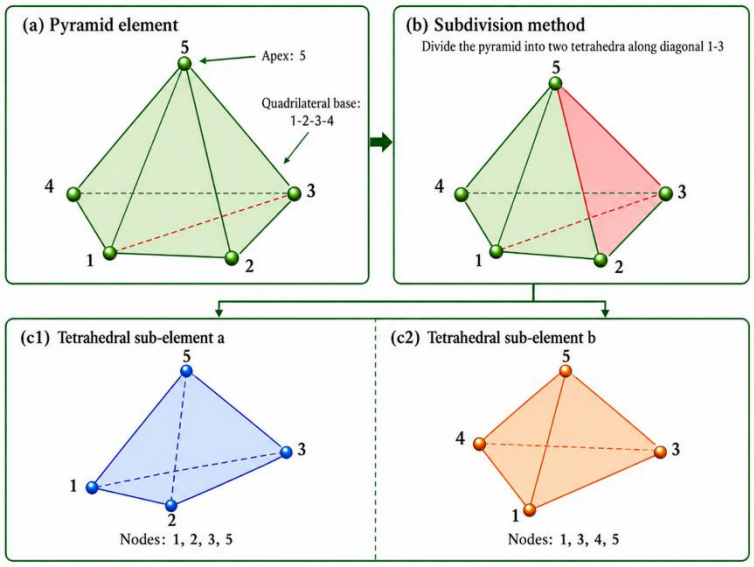



**Fig. 4.** Schematic of equivalent decomposition of a pyramid element into two tetrahedral sub-elements.

## 2.4 Volume-Weighted Density Filtering Method

The hybrid mesh generation strategy and the treatment of pyramid transition elements can ensure conformal connectivity between different mesh regions. However, during density filtering, substantial differences in element volume arise among different mesh types. Tetrahedral elements employed in transition regions and near complex boundaries are generally much smaller than the hexahedral elements used in other regular interior regions.

Conventional density filtering constructs a weighted average over neighboring elements primarily according to the distances between their centroids [24]. This approach performs well for regular structured meshes, in which the element volumes are nearly uniform and neighboring elements therefore represent approximately equal portions of the physical domain [25]. However, for hybrid mesh, distance-based smoothing of the design variables may be disproportionately influenced by the local number and spatial distribution of small-volume elements. Consequently, the contribution of each element becomes inconsistent with the physical volume it represents, thereby compromising the physical consistency of the filtered density field.

The conventional density filtering scheme is expressed as follows:

$$\widetilde{x_e} = \frac{\sum_{i \in N_e} H_{ei}\, x_i}{\sum_{i \in N_e} H_{ei}} \tag{2}$$

where $x_i$ denotes the unfiltered design variable of neighboring element $i$, $\widetilde{x_e}$ is the filtered design variable of element $e$, $N_e$ represents the set of neighboring elements located within the filter radius of element $e$, and $H_{ei}$ denotes the filtering weight coefficient between element $e$ and $i$, which is commonly defined as:

$$H_{ei} = max(0, R_{min} - d_{ei}) \tag{3}$$

where $R_{min}$ denotes the filter radius, and $d_{ei}$ represents the Euclidean distance between the centroids of elements $e$ and $i$.

To demonstrate the necessity of volume-weighted density filtering, a hybrid-mesh model with a pronounced difference in element volume was reconstructed based on the model presented in Section 2.1, as shown in Fig. 5. The characteristic edge length of the hexahedral elements was set to twice that of the tetrahedral elements. Statistical analysis showed that the average volumes of the hexahedral and tetrahedral elements were 0.512mm$^3$ and 0.076mm$^3$, respectively, corresponding to a volume ratio of approximately 6.74. When the conventional density filtering scheme was employed, pronounced density stratification appeared in the optimized topology, as shown in Fig. 6(a). This result indicates that conventional distance-based density filtering has limited capability in handling hybrid meshes containing elements with substantial volume differences.

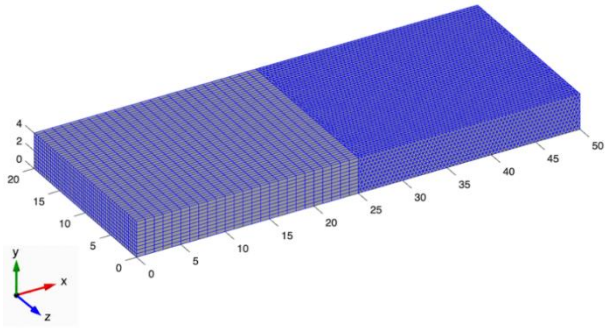
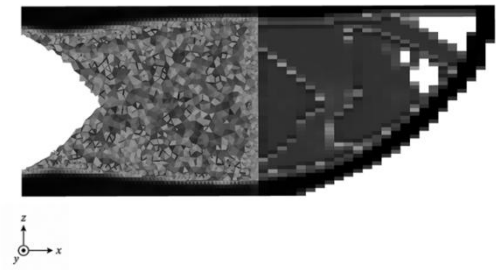
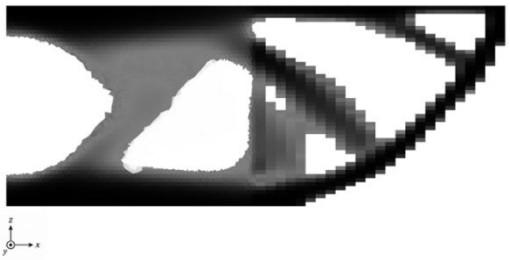



**Fig. 5.** Hybrid Mesh Model with Significant Differences in Element Volume.



(a) Topology optimization result of the cantilever beam with conventional density filtering



(b) Topology optimization result of the cantilever beam with volume-weighted density filtering

**Fig. 6.** Topology optimization results using conventional and volume-weighted density filters.

To address the aforementioned issue, a volume-weighted density filtering method suitable for three-dimensional mixed meshes, as illustrated in Fig. 7, is introduced into the conventional density filtering scheme.

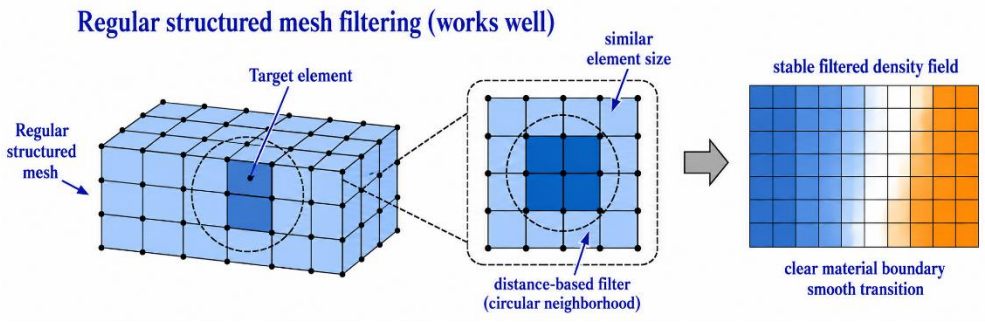
By simultaneously accounting for the centroid distance and physical volume of neighboring elements, the proposed method captures both their spatial proximity and their actual volumetric contributions to the design domain. Consequently, the rationality and numerical stability of density-field updating in hybrid meshes are improved. The corresponding discrete formulation is modified as follows:

$$\widetilde{x_e} = \frac{\sum_{i \in N_e} H_{ei} V_i x_i}{\sum_{i \in N_e} H_{ei} V_i} \tag{4}$$

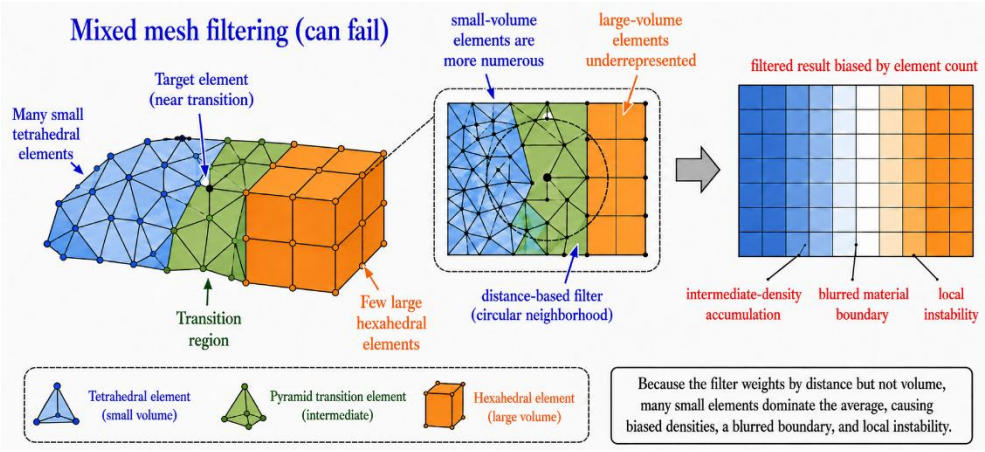
where $V_i$ denotes the actual physical volume of element $i$.
According to the chain rule, the sensitivity of the objective function with respect to the unfiltered design variables can be expressed as:

$$\frac{\partial J}{\partial x_e} = \sum_{i \in I_e} \frac{H_{ie} V_e}{\sum_{j \in N_i} H_{ij} V_j} \frac{\partial J}{\partial \tilde{x}_i} \tag{5}$$

Accordingly, the element volume participates not only in the density filtering process but also in determining the transfer weights of sensitivities within the filtering neighborhood. This enables the optimization iterations to more accurately reflect the actual spatial contributions of different elements in the hybrid mesh. As shown in Fig. 6(b), compared with the conventional density filtering method, the volume-weighted density filtering method produces a clearer material distribution, more distinct structural boundaries, and a more reliable optimized topology.




(a)Regular structured mesh filtering




(b)Mixed mesh filtering

**Fig. 7.** Schematic illustration of the volume-weighted density filtering method.

## 3. Topology Optimization Model under Time-Varying Loads

### 3.1 Formulation of the Topology Optimization Model

To describe the material distribution within the design domain, a variable-density-based topology optimization method is adopted. The design domain is discretized into finite elements, and each element is assigned a continuous density design variable $x_e$,

whose admissible range is defined as： $0 < x_{min} \le x_e \le 1, e = 1,2,\ldots,N_e$, where $x_{min}$ denotes the minimum allowable density introduced to prevent singularity of the global stiffness matrix.

For the transient dynamic response of a structure subjected to time-varying loads, the minimization of the transient compliance over the entire time interval is selected as the optimization objective. Accordingly, the topology optimization problem is formulated as follows:

$$\begin{aligned} &\min_{x} J \\ \text{s.t.} \quad &\frac{\sum_{e=1}^{N_e} x_e V_e}{\sum_{e=1}^{N_e} V_e} \le V^* \\ &x_{min} \le x_e \le 1, \end{aligned} \tag{6}$$

where $J$ denotes the transient compliance objective function, $V_e$ is the volume of element $e$, and $V^*$ represents the prescribed volume fraction constraint.

To characterize the overall structural response under dynamic loading, the transient compliance accumulated over the prescribed time interval is adopted as the optimization objective function. Its continuous form is expressed as:

$$J = \int_0^T u^T(t) F(t)\, dt \tag{7}$$

For numerical implementation, the time domain is discretized into a series of discrete time steps, and the Eq.（7）expression can be rewritten as:

$$J \approx \sum_{t=1}^{N_t} u^T(t) \boldsymbol{F}(t)\, \Delta t \tag{8}$$

where $J$ denotes the objective function, $T$ is the total duration of the transient analysis, $u(t)$ represents the structural displacement response vector at time $t$, $F(t)$ denotes the external load vector at time $t$, $N$ is the total number of time steps, and $\Delta t$ is the time-step size.

To establish the relationship between the design variables and the structural stiffness and mass, the solid isotropic material with penalization (SIMP) model is adopted. Accordingly, the elastic modulus and material density of each element are interpolated as functions of the corresponding design variable:

Interpolation of the element elastic modulus and material density:

$$E_e = E_{min} + x_e^p (E_0 - E_{min}), \qquad \rho_e = \rho_{min} + x_e^p (\rho_0 - \rho_{min}) \tag{9}$$

where $E_e$ and $\rho_e$ denote the interpolated elastic modulus and material density of element $e$, respectively; $E_0$ and $\rho_0$ are the elastic modulus and material density of the solid material, respectively; $E_{min}$ and $\rho_{min}$ are small positive lower bounds introduced to prevent singularity of the global stiffness and mass matrices; and $p$ is the penalization factor used to suppress intermediate densities and promote a clear solid–void boundary.

Based on the material interpolation relationships given in Eq. (9), the element stiffness $K_e$ and mass matrices $M_e$ can be further expressed as:

$$K_e(x_e) = \left[E_{min} + x_e^p (E_0 - E_{min})\right] K_e^*, M_e(x_e) = \left[\rho_{min} + x_e^p (\rho_0 - \rho_{min})\right] M_e^* \tag{10}$$

where $K_e^*$ and $M_e^*$ denote the reference element stiffness and mass matrices corresponding to unit elastic modulus and unit material density, respectively. In

gradient-based topology optimization, the design variables are updated according to the derivatives of the objective and constraint functions with respect to the design variables. Therefore, after interpolating the material properties, the derivatives of the element stiffness and mass matrices with respect to the design variable $x_e$ must also be evaluated. These derivatives provide the basis for the subsequent sensitivity analysis of the transient compliance objective function. Differentiating the interpolation relationships given in Eq. (10) with respect to $x_e$ yields:

$$\frac{\partial E_e}{\partial x_e} = p x_e^{p-1}(E_0 - E_{min}), \frac{\partial \rho_e}{\partial x_e} = p x_e^{p-1}(\rho_0 - \rho_{min}) \tag{11}$$

The derivatives of the element stiffness and mass matrices with respect to the design variable can then be expressed as:

$$\frac{\partial K_e}{\partial x_e} = p x_e^{p-1}(E_0 - E_{min})K_e^*, \frac{\partial M_e}{\partial x_e} = p x_e^{p-1}(\rho_0 - \rho_{min})M_e^* \tag{12}$$

In this section, the parametric relationships among the design variables, material properties, and element system matrices have been established, together with the corresponding matrix derivative expressions. These formulations provide the theoretical basis for the transient dynamic response analysis and the subsequent sensitivity analysis. The following section presents the solution procedure for the transient dynamic response of structures subjected to time-varying loads.

### 3.2 Transient Dynamic Analysis

Under time-varying loads, the structural response evolves continuously with time, and the displacement, velocity, and acceleration exhibit pronounced transient characteristics. Unlike static analysis, which considers only the equilibrium state of the structure, transient dynamic analysis must also account for inertial and damping effects. Therefore, to determine the structural response at each time step and provide the response quantities required for the subsequent evaluation of transient compliance and sensitivity analysis, a transient dynamic analysis is performed.

The spatially discretized equation of motion can be expressed as:

$$M\ddot{u}(t) + C\dot{u}(t) + Ku(t) = F(t) \tag{13}$$

where $M$、$C$、$K$ denote the global mass, damping, and stiffness matrices, respectively; $\ddot{u}(t)$、$\dot{u}(t)$、$u(t)$ represent the acceleration, velocity, and displacement response vectors, respectively; and $F(t)$ is the time-varying external load vector.

To account for the influence of structural damping on the transient response, the global damping matrix is constructed by using the Rayleigh damping model:

$$C = \alpha M + \beta_r K \tag{14}$$

where $\alpha$ and $\beta_r$ denote the mass-proportional and stiffness-proportional damping coefficients, respectively.

Because Eq. (13) is a second-order differential equation that evolves with time, a time-integration scheme is required to determine the structural response successively at each discrete time instant. In this study, the Newmark method [26] is adopted for temporal discretization. By approximating the displacement, velocity, and acceleration within each time step, the method transforms the governing differential equation into a sequence of algebraic equations. Within the time interval $t \to t + \Delta t$, the displacement and velocity update equations of the Newmark method are given by:

$$u_{t+\Delta t} = u_t + \Delta t \dot{u}_t + \frac{\Delta t^2}{2}\left[(1-2\beta)\ddot{u}_t + 2\beta \ddot{u}_{t+\Delta t}\right] \tag{15}$$

$$\dot{u}_{t+\Delta t} = \dot{u}_t + \Delta t\left[(1-\gamma)\ddot{u}_t + \gamma \ddot{u}_{t+\Delta t}\right] \tag{16}$$

where $\beta$ and $\gamma$ are the Newmark integration parameters. In this study, $\beta = 1/4$ and $\gamma = 1/2$ are adopted. With these values, the average acceleration scheme is unconditionally stable for linear structural systems and is therefore suitable for transient dynamic response analysis.

From the Eq. (16), the update for acceleration and velocity can be further expressed as:

$$\ddot{u}_{t+\Delta t} = a_0(u_{t+\Delta t} - u_t) - a_2 \dot{u}_t - a_3 \ddot{u}_t \tag{17}$$

$$\dot{u}_{t+\Delta t} = \dot{u}_t + a_6 \ddot{u}_t + a_7 \ddot{u}_{t+\Delta t} \tag{18}$$

Substituting the Newmark update equations into the governing equation of motion yields the following equivalent linear system at each time step:

$$K_{eff} u_{t+\Delta t} = R_t \tag{19}$$

The effective stiffness matrix and effective load vector are given by：

$$K_{eff} = K + a_0 M + a_1 C \tag{20}$$

$$R_t = F_{t+\Delta t} + M(a_0 u_t + a_2 \dot{u}_t + a_3 \ddot{u}_t) + C\left(a_{1u_t} + a_4 \dot{u}_t + a_5 \ddot{u}_t\right) \tag{21}$$

where $a_0 = \frac{1}{\beta \Delta t^2}; a_1 = \frac{\gamma}{\beta \Delta t}; a_2 = \frac{1}{\beta \Delta t}; a_3 = \frac{1}{2\beta} - 1; a_4 = \frac{\gamma}{\beta} - 1; a_5 = \frac{\Delta t}{2}\left(\frac{\gamma}{\beta} - 2\right)$

$$a_6 = \Delta t(1-\gamma); a_7 = \gamma \Delta t$$

In summary, by using the Newmark time integration method, the transient dynamic governing equations can be transformed into a sequence of algebraic equations to be solved at each time step. Consequently, the displacement, velocity, and acceleration responses throughout the entire analysis period can be efficiently obtained. These transient response quantities provide the basis for evaluating the transient compliance objective and its sensitivities, thereby laying the foundation for the subsequent design-variable update and transient dynamic topology optimization.

## 4. Numerical Implementation and Algorithmic Procedure

### 4.1 Assembly of the Global Stiffness Matrices

To enable the unified treatment of different element types within a common finite element framework, the elements in the hybrid mesh are automatically identified and classified according to their nodal topology. The program first reads the element connectivity information and determines the corresponding element type based on the number of element nodes. The appropriate element-level computational routine is then invoked to evaluate the stiffness and mass matrices for each element. Subsequently, the global matrices are assembled through the mapping between the element degrees of freedom and the global degrees of freedom, thereby establishing a finite element discretization framework suitable for hybrid-mesh structures.

For an arbitrary three-dimensional solid element, the general forms of the element stiffness matrix $\mathbf{K}_\mathrm{e}$ and consistent mass matrix $\mathbf{M}_\mathrm{e}$ are expressed as [20,27]:

$$\mathbf{K}_\mathrm{e} = \int_{\Omega_\mathrm{e}} \mathbf{B}_\mathrm{e}^\mathrm{T}\, \mathbf{D}\mathbf{B}_\mathrm{e}\, d\Omega \tag{24}$$

$$\boldsymbol{M}_e = \int_{\Omega_\mathrm{e}} \rho\, \mathbf{N}_\mathrm{e}^\mathrm{T}\mathbf{N}_\mathrm{e}\, d\Omega \tag{25}$$

where $\Omega_e$ denotes the integration domain of the $e$-th element, $\mathbf{B}_e$ is the strain–displacement matrix, $\mathbf{D}$ is the constitutive matrix of the material, $\mathbf{N}_e$ represents the element shape-function matrix, and $\rho$ is the material density. The primary differences among various element types lie in the formulation of the shape functions, the coordinate mapping, and the numerical integration scheme.

(1) Tetrahedral element

For the four-node linear tetrahedral element, the displacement field is interpolated by using linear shape functions. Since the first-order derivatives of the linear shape functions with respect to the physical coordinates remain constant throughout the element, the corresponding strain–displacement matrix $\mathbf{B}_e$ is constant within the element. Accordingly, the element stiffness matrix can be obtained from Eq. (24) as

$$\mathbf{K}_e = \mathbf{B}_e^T \mathbf{D}\mathbf{B}_e \cdot V \tag{26}$$

where $\mathbf{B}_e$ is the strain–displacement matrix, $\mathbf{D}$ is the material constitutive matrix, and $V$ denotes the element volume.

(2) Hexahedral element

For the eight-node hexahedral element, the displacement field is interpolated by using trilinear shape functions. Since the Jacobian matrix and the corresponding strain–displacement matrix varies within the element, the element matrices cannot be evaluated analytically in a straightforward manner and should instead be computed by using numerical integration. In this study, a $2 \times 2 \times 2$ Gauss quadrature scheme is adopted. The corresponding element stiffness matrix and consistent mass matrix are expressed as:

$$\mathbf{K}_e = \sum_{i=1}^{2}\sum_{j=1}^{2}\sum_{k=1}^{2} \mathbf{B}_{ijk}^T \mathbf{D}\mathbf{B}_{ijk} \left|\det(\mathbf{J}_{ijk})\right| w_i w_j w_k \tag{27}$$

$$\mathbf{M}_e = \rho \sum_{i=1}^{2}\sum_{j=1}^{2}\sum_{k=1}^{2} \mathbf{N}_{ijk}^T \mathbf{N}_{ijk} \left|\det(\mathbf{J}_{ijk})\right| w_i w_j w_k \tag{28}$$

where $\mathbf{J}_{ijk}$ denotes the Jacobian matrix evaluated at the Gauss integration point in the natural coordinate system, while $\mathbf{B}_{ijk}$ and $\mathbf{N}_{ijk}$ are the corresponding strain–displacement matrix and shape-function matrix, respectively. The quantities $w_i$, $w_j$, and $w_k$ denote the Gauss quadrature weights along the three natural-coordinate directions. For the standard two-point Gauss quadrature, the integration points in each natural-coordinate direction are located at $\pm\frac{1}{\sqrt{3}}$, with all corresponding quadrature weights equal to unity.

(3) Pyramid element

To ensure a consistent computational formulation within the hybrid-mesh finite element framework, each five-node pyramid transition element is subdivided into two tetrahedral subelements according to its nodal topology prior to the evaluation of the element matrices. The stiffness and mass matrices of the two tetrahedral subelements are then computed separately. Subsequently, the subelement matrices are assembled through a consistent mapping of the nodal degrees of freedom to obtain the equivalent stiffness and mass matrices of the pyramid element, thereby allowing the pyramid element to be treated within the same computational framework as the tetrahedral element. After the stiffness matrices of all elements have been evaluated, they are assembled into the global stiffness matrix through the mapping between the element and global degrees of freedom:

$$\mathbf{K} = \sum_{e=1}^{N_e} \mathbf{K}_e \,, \mathbf{M} = \sum_{e=1}^{N_e} \mathbf{M}_e \,, \mathbf{C} = \sum_{e=1}^{N_e} \mathbf{C}_e \tag{29}$$

where $N_e$ is the total number of elements; $\mathbf{K}_e$, $\mathbf{M}_e$, and $\mathbf{C}_e$ denote the stiffness, mass, and damping matrices of the $e$-th element, respectively; and $\mathbf{K}$, $\mathbf{M}$, and $\mathbf{C}$ are the assembled global stiffness, mass, and damping matrices, respectively.

During the numerical evaluation of the element matrices, finite-precision arithmetic associated with floating-point operations, numerical integration, and matrix assembly may introduce slight asymmetry into the stiffness, mass, and damping matrices, although these matrices are theoretically symmetric. To restore their symmetry and improve the numerical stability of the subsequent solution procedure, the matrices are symmetrized as follows:

$$\mathbf{K} = \frac{1}{2}(\mathbf{K} + \mathbf{K}^T), \mathbf{M} = \frac{1}{2}(\mathbf{M} + \mathbf{M}^T), \mathbf{C} = \frac{1}{2}(\mathbf{C} + \mathbf{C}^T) \tag{30}$$

4.2 Transient Sensitivity Analysis and Optimization Iteration

After assembling the global system matrices, the transient dynamic response is obtained by using the Newmark time integration scheme described in Section 3.2. At each time step, the discretized equation of motion can be expressed as：

$$\mathbf{K}_{eff} u_{t+\Delta t} = \mathbf{R}_t \tag{31}$$

where $\mathbf{R}_t$is the effective load vector determined by the external load together with the displacement, velocity, and acceleration at the current time step; $\mathbf{K}_{eff}$ is the effective stiffness matrix, i.e.,

$$\mathbf{K}_{eff} = \mathbf{K} + a_0\mathbf{M} + a_1\mathbf{C} \tag{32}$$

The explicit expression of $\mathbf{K}_{eff}$ is presented in Section 3.2.

For each time step, the transient response is computed according to the following procedure:

（1）Construct the effective load vector $\mathbf{R}_t$based on the displacement, velocity, and acceleration at the current time step;

（2）Solve the linear system to obtain the displacement vector $\mathbf{u}_{t+\Delta t}$at the next time step;

（3）Update the velocity and acceleration by using the Newmark recurrence equations;

（4）Advance to the next time step and repeat the procedures (1)-(3)until the entire time history is completed.

The overall time-stepping procedure is summarized in Fig. 8.

Through the above time-stepping procedure, the transient responses of the structure, including the displacement, velocity, and acceleration histories, are obtained over the entire analysis period. Based on these transient response quantities, the sensitivity of the objective function with respect to the design variables is subsequently evaluated to provide the gradient information required for topology optimization. In this study, the transient compliance is adopted as the objective function, and its discrete form is given by

$$J = \sum_{t=1}^{N_t} u_t^T F_t \ \Delta t \tag{33}$$

where $\mathbf{u}_t$ is the displacement vector at the $t$-th time step, $\mathbf{F}_t$ denotes the external load vector, and $N_t$ is the total number of time steps. The objective function characterizes the overall structural response to the applied external loads over the entire time domain. During the transient dynamic analysis, the dynamic equilibrium equation (Eq. (13)) is satisfied at every time step. Accordingly, for the design variable $x_e$associated with the $e$-th element, the derivative of the objective function with respect to $x_e$ can be expressed as:

$$\frac{\partial J}{\partial x_e} = -\int_0^T \frac{\partial u^{\mathrm{T}}}{\partial x_e} F(t)dt + \int_0^T U^T(t) \frac{\partial F}{\partial x_e} dt \tag{34}$$

The sensitivity expression can therefore be obtained as follows [28]:

$$\frac{\partial J}{\partial x_e} = -\int \left( u_t^T \frac{\partial K}{\partial x_e} u_t + u_t^T \frac{\partial C}{\partial x_e} \dot{u}_t + u_t^T \frac{\partial M}{\partial x_e} \ddot{u}_t \right) dt \tag{35}$$

The discrete form of the sensitivity expression is given by:

$$\frac{\partial J}{\partial x_e} \approx -\sum_{t=1}^{N_t} \Delta t \left( u_t^T \frac{\partial K}{\partial x_e} u_t + u_t^T \frac{\partial C}{\partial x_e} \dot{u}_t + u_t^T \frac{\partial M}{\partial x_e} \ddot{u}_t \right) \tag{36}$$

The three terms on the right-hand side, as given in Eqs. (34) – (36), represent the contributions of the stiffness, damping, and mass matrices, respectively. thereby characterizing the effects of different physical mechanisms on the objective function during the transient dynamic response.

Once the sensitivity of the objective function with respect to the design variables has been obtained, the Method of Moving Asymptotes (MMA) [29] is employed to transform the original nonlinear optimization problem into a sequence of computationally tractable convex subproblems, providing favorable convergence and numerical stability.

At the $k$-th optimization iteration, the design variables are updated as:

$$x^{k+1} = \mathrm{MMA}\left(x^k, \frac{\partial J}{\partial x}\right) \tag{37}$$

where $\mathbf{x}^k$ and $\mathbf{x}^{k+1}$ denote the design-variable vectors at the $k$-th and $(k+1)$-th iterations, respectively, and $\frac{\partial J}{\partial x}$ represents the gradient of the objective function at the current iteration.

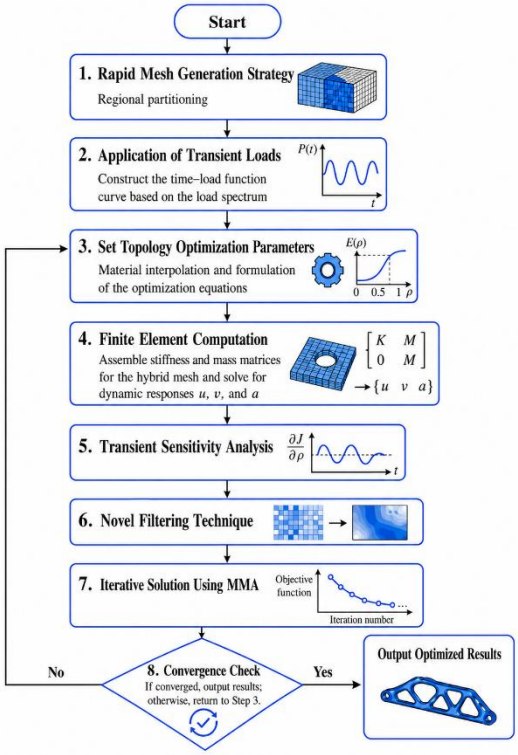


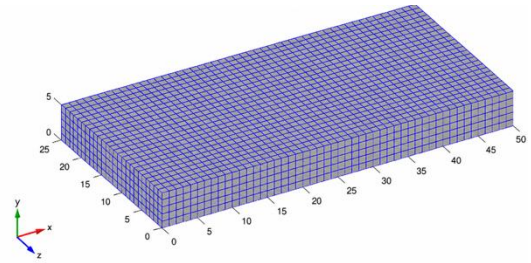

**Fig. 8.** Flowchart of topology optimization under time-varying loads.

## 5. Examples

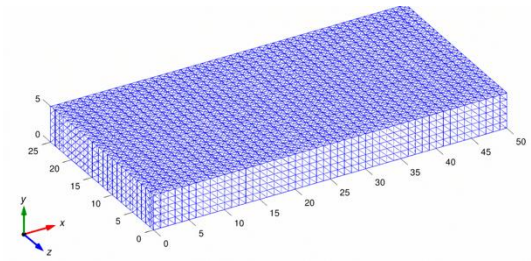
## 5.1 Design of Comparative Cases for the Basic Numerical Example

To evaluate the effectiveness of the proposed topology optimization method and establish a reference benchmark for the subsequent hybrid-mesh examples, the cantilever beam introduced in Section 2.1 is employed as a standard test case. The design domain is discretized separately by using hexahedral and tetrahedral meshes. By comparing the optimized topologies, material distributions, and primary load-transfer paths obtained by using the two single-mesh discretization schemes, a reference is provided for assessing the rationality and numerical stability of the subsequent hybrid-mesh topology optimization results[30,31].

As shown in Fig. 9, under identical loading and boundary conditions, both mesh discretization schemes produce well-defined primary load-transfer paths. The optimized material is primarily distributed near the fixed end, the loading region, and the inclined supporting members connecting these two regions. The overall topological configurations obtained by using the two element types exhibit good agreement at the macroscopic level, indicating that this example is suitable as a benchmark for validating the proposed hybrid-mesh method. Nevertheless, owing to differences between tetrahedral and hexahedral elements in their element stiffness formulations, numerical integration schemes, and geometric discretization characteristics, minor discrepancies are observed along local boundaries and in fine structural features. These discrepancies represent normal numerical deviations arising from the use of different discretization schemes.



(a) Hexahedral mesh of the cantilever beam



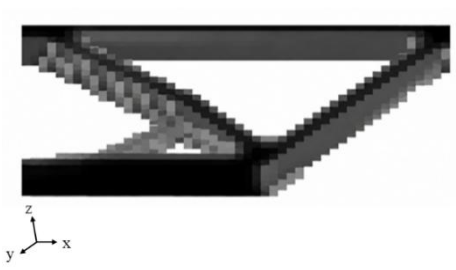
(b) Tetrahedral mesh of the cantilever beam



(c) Front view of the optimization result with hexahedral mesh



(d) Front view of the optimization result with tetrahedral mesh




(e) Isometric view of the optimization result with hexahedral meshes

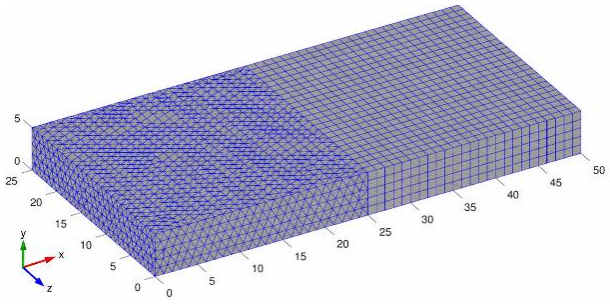



(f) Isometric view of the optimization result with tetrahedral meshes

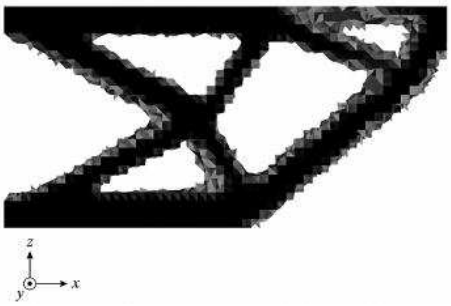
**Fig. 9.** Comparison of topology optimization results obtained by different mesh discretization schemes.

## 5.2 Design and Comparative Analysis of Hybrid-Mesh Topology Optimization Cases

In this example, the geometry of the design domain, boundary conditions, and applied load are identical to those used in the standard numerical example presented in Section 5.1. To verify the applicability of the hybrid-mesh discretization method to topology optimization, the design domain is discretized by using a conforming hybrid mesh composed of tetrahedral and hexahedral elements. Pyramid elements are introduced in the transition region between the two mesh types to ensure a conforming connection. [32,33]The resulting hybrid-mesh discretization and corresponding optimized topology are presented in Fig. 10.




(a) Hybrid mesh of the cantilever beam




(b) Front view of the optimization result with hybrid mesh




(c) Isometric view of the optimization result with hybrid mesh

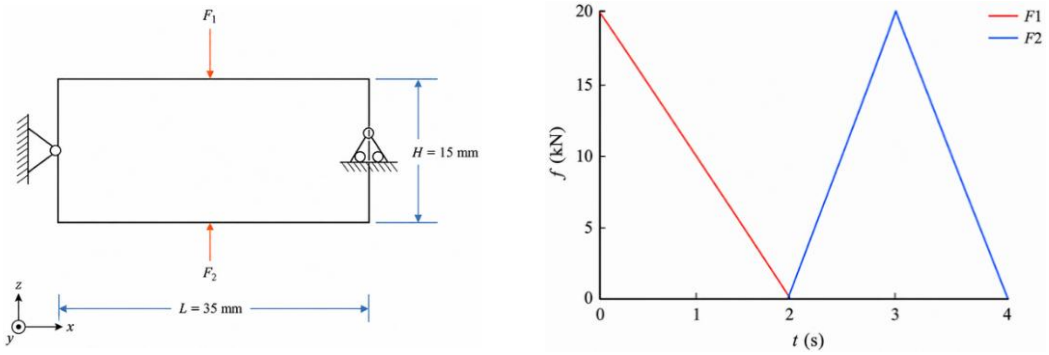
**Fig. 10.** Topology Optimization Result of the Cantilever Beam with Hybrid Meshes.

A comparison between the hybrid-mesh topology optimization results and the benchmark results presented in Section 5.1 shows good agreement in terms of the overall material distribution, primary load-transfer paths, and global topological configuration. Minor discrepancies are observed only in local structural details, which fall within the range of acceptable numerical errors introduced by different mesh discretization schemes. These results demonstrate that the proposed hybrid-mesh discretization strategy effectively preserves the accuracy, stability, and reliability of the topology optimization while providing the geometric flexibility required for complex structural discretization.

## 5.3 Design and Comparative Analysis of Topology Optimization Cases under Time-Varying Loads

In this section, time-varying loads are introduced into the benchmark simply supported beam problem to investigate the transient dynamic topology optimization of regular structures. This example is employed to validate the applicability of the proposed topology optimization model under time-varying loading conditions. A simply supported beam is selected as the benchmark structure, whose geometry and mesh discretization are shown in Figs. 11 and 12, respectively.[34,35]

For the loading conditions, load $F_1$ is applied at the designated location on the upper surface of the structure, whereas load $F_2$ is applied at the designated location on the lower surface. Both loading cases follow piecewise linear loading histories. Transient dynamic topology optimization is performed separately for the two loading scenarios, and the corresponding optimized topologies are presented in Table1.




(a) The geometry of a simply supported beam

(b) Time-varying loading history

**Fig. 11.** Simply supported beam and the applied time-varying load.

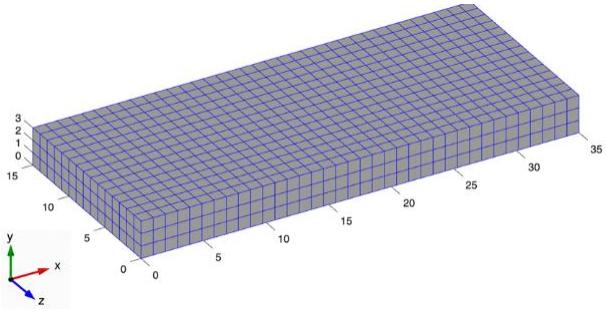
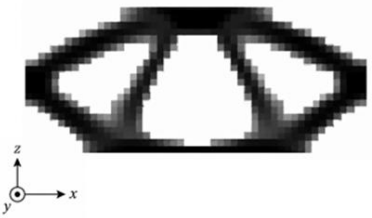



**Fig. 12.** Mesh discretization for the simply supported beam.

**Table1**

Topology results for structural dynamics cases.

| T(s) | Configurations |
|---|---|
| 1 |  |
| 2 |  |
| 3 |  |
| 4 |  |

From the comparison of the optimization results for the cases in Table 1 in this section, it is evident that the topology optimization results of structures subjected to time-varying loads depend not only on the load positions but also on the load time-history features. During the first 2s of loading, the loading direction remains unchanged, resulting in a continuously increasing accumulated impulse. Under this condition, the loading effect can be approximately regarded as an equivalent static load acting in the same direction, and the resulting optimized topology is therefore consistent with that obtained from static topology optimization, exhibiting an overall symmetric configuration.

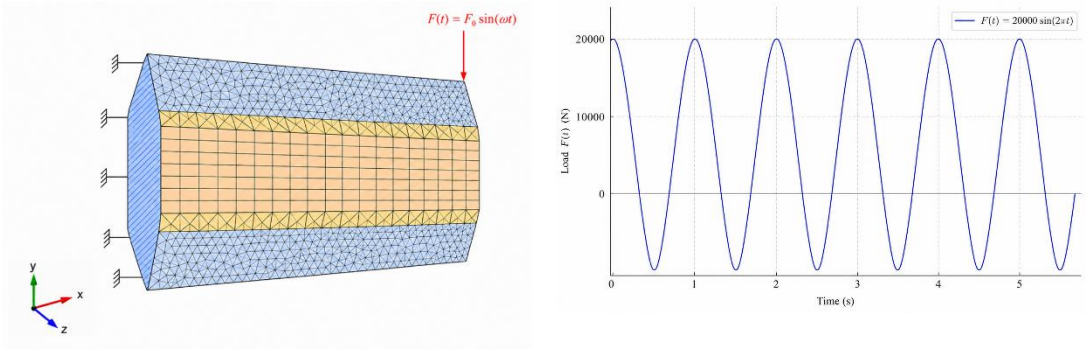
As the loading duration increases to 3 s, the load reverses its direction. However, since the positive and negative impulses have not yet completely canceled each other, the accumulated impulse becomes asymmetric, giving rise to a directional transient dynamic response. Consequently, the optimized topology exhibits a pronounced asymmetric material distribution. When the loading duration reaches 4 s, the positive and negative impulses are fully balanced, causing the accumulated impulse to return to zero. As a result, the overall transient dynamic response becomes symmetric again, and the optimized topology recovers a symmetric configuration.

These results indicate that the optimized topology obtained from transient dynamic topology optimization is strongly dependent on the loading history. The final material distribution is determined not only by the loading magnitude and application location but also by the accumulated impulse and the evolution of the transient dynamic response throughout the loading process.

## 5.4 Hybrid-Mesh Topology Optimization Cases under Time-Varying Loads

This section further investigates the topology optimization of a complex structure subjected to time-varying loads using the proposed hybrid-mesh framework. A wing-shaped structure, as shown in Fig. 13, is selected as the numerical example. Owing to its highly irregular geometric features, the regions with large curvature near the wing tips are discretized using tetrahedral elements to improve geometric adaptability, whereas the relatively regular central region is discretized using hexahedral elements to enhance computational accuracy and efficiency. The two types of elements are connected through transition elements to form a conforming hybrid-mesh model. For the boundary conditions, the left end face of the structure is fully constrained, while a sinusoidal time-varying load is applied at the designated location on the upper surface to simulate transient dynamic loading. This example is employed to further assess the applicability and numerical stability of the proposed hybrid-mesh topology optimization method under the combined effects of complex geometry and time-varying loads.

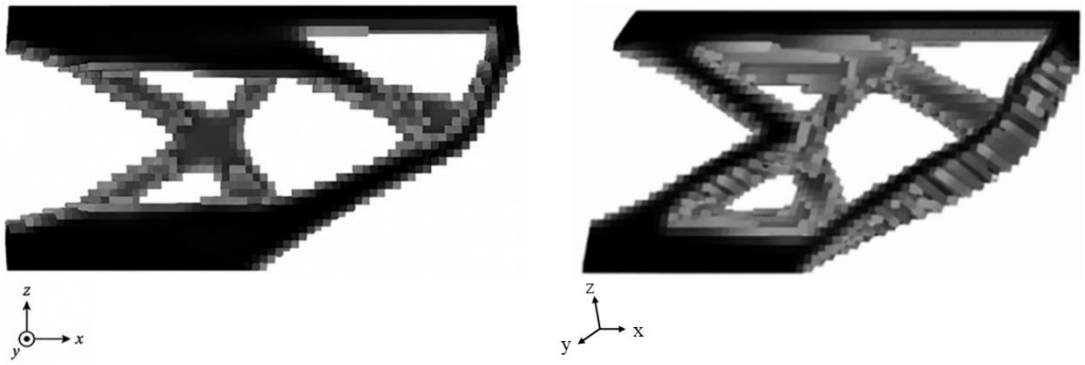
Fig. 14 presents the optimized topology obtained under the transient loading condition. It can be observed that the proposed hybrid-mesh approach successfully generates a clear primary load-transfer path, with material predominantly distributed in the critical load-bearing regions. The resulting topology is consistent with the structural load-transfer characteristics, demonstrating the effectiveness, robustness, and engineering applicability of the proposed method for transient dynamic topology optimization of complex three-dimensional structures.




(a) Schematic of the complex structure

(b) Loading conditions of the complex structure

**Fig. 13.** Schematic of the wing-shaped structure.




(a) Front view of the topology optimization result

(b) Isometric view of the topology optimization result

**Fig. 14.** Topology optimization results for the complex structure.

## 6. Conclusions

A transient dynamic topology optimization framework based on hybrid meshes is proposed to overcome the limitations of conventional single-mesh discretization in terms of geometric adaptability and computational efficiency for complex structures subjected to time-varying loads. Correspondingly, the effectiveness and applicability of the proposed method were systematically investigated. The main conclusions are as follows:

(1) For complex three-dimensional structures, a hybrid-mesh discretization and unified finite element computation framework is proposed to address the inconsistency in the computational treatment of different element types in hybrid-mesh topology optimization. within terms of pyramid transition elements among the hybrid-meshes , an equivalent decomposition strategy is presented to enable the unified computation and assembly of different types of elements within a common finite element framework, thereby improving the computational stability and engineering applicability of hybrid-mesh topology optimization for complex structures.

(2) A topology optimization model based on transient dynamic response was established by coupling the structural dynamic equilibrium equations with the variable-

density method. The transient compliance under time-varying loads was employed as the optimization objective, and the corresponding sensitivity formulation with respect to the design variables was derived. The proposed formulation enables the optimization process to simultaneously account for the influences of structural stiffness, damping, and inertia on the transient dynamic response.

(

(3) To eliminate the filtering bias caused by the significant volume differences among different element types in hybrid meshes, a volume-weighted density filtering method was proposed. By introducing the actual physical volume of each element into the conventional distance-based filtering scheme, the proposed method simultaneously considers spatial proximity and volumetric contribution during density filtering. Numerical results demonstrate that the proposed filter effectively suppresses the nonphysical influence arising from the numerical dominance of small-volume elements on the update of density field and improve the density continuity in hybrid mesh transition regions.

(4) The proposed hybrid-mesh-based transient dynamic topology optimization method improves the geometric modeling capability for complex structures while maintaining computational accuracy and effectively capturing the influence of time-varying loads on structural topology evolution. The proposed framework provides a promising approach for lightweight design and dynamic structural optimization of complex three-dimensional engineering structures.

## Acknowledgements

The authors would like to thank the support of the National Natural Science Foundation of China (Grant No. 52475169).

## 7. References


[1] MUKHERJEE S, LU D, RAGHAVAN B, et al. Accelerating large-scale topology optimization: State-of-the-art and challenges[J]. Archives of Computational Methods in Engineering, 2021, 28(7): 4549–4571. DOI: 10.1007/s11831-021-09544-3.

[2] QUERIN O M, YOUNG V, STEVEN G P, et al. Computational efficiency and validation of bi-directional evolutionary structural optimisation[J]. Computer Methods in Applied Mechanics and Engineering, 2000, 189(2): 559–573. DOI: 10.1016/S0045-7825(99)00309-6.

[3] TANG T, WANG L, ZHU M, et al. Topology optimization: A review for structural designs under statics problems[J]. *Materials*, 2024, 17(23): 5970. DOI: 10.3390/ma17235970.

[4] SIGMUND O. A 99 line topology optimization code written in Matlab[J]. *Structural and Multidisciplinary Optimization*, 2001, 21(2): 120–127.

[5] ANDREASSEN E, CLAUSEN A, SCHEVENELS M, et al. Efficient topology optimization in MATLAB using 88 lines of code[J]. *Structural and Multidisciplinary Optimization*, 2011, 43: 1–16. DOI: 10.1007/s00158-010-0594-7.

[6] TALISCHI C, PAULINO G H, PEREIRA A, et al. PolyTop: A Matlab implementation of a general topology optimization framework using unstructured polygonal finite element meshes[J]. *Structural and Multidisciplinary Optimization*, 2012, 45(3): 329–357. DOI: 10.1007/s00158-011-0696-x.

[7] LIU K, TOVAR A. An efficient 3D topology optimization code written in Matlab[J]. *Structural and Multidisciplinary Optimization*, 2014, 50: 1175–1196. DOI: 10.1007/s00158-014-1107-x.

[8] FERRARI F, SIGMUND O. A new generation 99 line Matlab code for compliance topology optimization and its extension to 3D[J]. *Structural and Multidisciplinary Optimization*, 2020, 62: 2211–2228. DOI: 10.1007/s00158-020-02629-w.

[9] GAO J, GAO L, LUO Z, et al. Isogeometric topology optimization for continuum structures using density distribution function[J]. *International Journal for Numerical Methods in Engineering*, 2019, 119: 991–1017. DOI: 10.1002/nme.6081.

[10] GAO J, WANG L, LUO Z, et al. IgaTop: An implementation of topology optimization for structures using IGA in MATLAB[J]. *Structural and Multidisciplinary Optimization*, 2021, 64: 1669–1700. DOI: 10.1007/s00158-021-02858-7.

[11] JIA Y, WANG C, ZHANG X S. FEniTop: A simple FEniCSx implementation for 2D and 3D topology optimization supporting parallel computing[J]. *Structural and Multidisciplinary Optimization*, 2024, 67: 140. DOI: 10.1007/s00158-024-03818-7.

[12] LI H, YAMADA T, JOLIVET P, et al. Full-scale 3D structural topology optimization using adaptive mesh refinement based on the level-set method[J]. *Finite Elements in Analysis and Design*, 2021, 194: 103561. DOI: 10.1016/j.finel.2021.103561.

[13] XU Z, WANG L, ZHAI X, et al. Voxel-to-tet meshing for density-based topology optimization[J]. *Computer Aided Geometric Design*, 2026, 128: 102567. DOI: 10.1016/j.cagd.2026.102567.
[14] MIN S, KIKUCHI N, PARK Y C, et al. Optimal topology design of structures under dynamic loads[J]. *Structural Optimization*, 1999, 17: 208–218.
[15] CHOI W S, PARK G J. Structural optimization using equivalent static loads at all time intervals[J]. *Computer Methods in Applied Mechanics and Engineering*, 2002, 191(19–20): 2105–2122.
[16] LEE H A, PARK G J. Nonlinear dynamic response topology optimization using the equivalent static loads method[J]. *Computer Methods in Applied Mechanics and Engineering*, 2015, 283: 956–970.
[17] CAO D, ZENG Y, MENG Z, et al. A transient dynamic topology optimization method with approximate dynamic response sensitivity using equivalent static loads[J]. *Computer Methods in Applied Mechanics and Engineering*, 2025, 436: 117760. DOI: 10.1016/j.cma.2025.117760.
[18] GUO Y, CHENG S, WANG Y, et al. Topology optimization for transient thermoelastic structures under time-dependent loads[J]. *Engineering with Computers*, 2024, 40: 1677–1693. DOI: 10.1007/s00366-023-01878-9.
[19] SAURABH S, GUPTA A, CHOWDHURY R, et al. Robust topology optimization for uncertainty in load positions of transient dynamic loading[J]. *Reliability Engineering & System Safety*, 2025, 264: 111440. DOI: 10.1016/j.ress.2025.111440.
[20] ZIENKIEWICZ O C, TAYLOR R L, ZHU J Z. *The Finite Element Method: Its Basis and Fundamentals*[M]. 7th ed. Oxford: Butterworth-Heinemann, 2013.
[21] SEVILLA R, HASSAN O, MORGAN K. The use of hybrid meshes to improve the efficiency of a discontinuous Galerkin method for the solution of Maxwell's equations[J]. *Computers & Structures*, 2014, 137: 2–13. DOI: 10.1016/j.compstruc.2013.01.014.
[22] BEDROSIAN G. Shape functions and integration formulas for three-dimensional finite element analysis[J]. *International Journal for Numerical Methods in Engineering*, 1992, 35(1): 95–108.
[23] OWEN S J, SAIGAL S. Formation of pyramid elements for hexahedra to tetrahedra transitions[J]. *Computer Methods in Applied Mechanics and Engineering*, 2001, 190(34): 4505–4518.
[24] BOURDIN B. Filters in topology optimization[J]. *International Journal for Numerical Methods in Engineering*, 2001, 50(9): 2143–2158. DOI: 10.1002/nme.116.
[25] GUEST J K, PRÉVOST J H, BELYTSCHKO T. Achieving minimum length scale in topology optimization using nodal design variables and projection functions[J]. *International Journal for Numerical Methods in Engineering*, 2004, 61(2): 238–254. DOI: 10.1002/nme.1064.
[26] NEWMARK N M. A method of computation for structural dynamics[J]. *Journal of the Engineering Mechanics Division, ASCE*, 1959, 85(EM3): 67–94. DOI: 10.1061/JMCEA3.0000098.

[27] STRANG G, FIX G J. *An Analysis of the Finite Element Method*[M]. Englewood Cliffs: Prentice-Hall, 1973.
[28] BEHROU R, GUEST J K. Topology optimization for transient response of structures subjected to dynamic loads[C]//*18th AIAA/ISSMO Multidisciplinary Analysis and Optimization Conference*. Denver, USA, 2017: 1–13. DOI: 10.2514/6.2017-3657.
[29] SVANBERG K. The method of moving asymptotes—A new method for structural optimization[J]. International Journal for Numerical Methods in Engineering, 1987, 24(2): 359–373. DOI: 10.1002/nme.1620240207.
[30] BENDSØE M P, KIKUCHI N. Generating optimal topologies in structural design using a homogenization method [J]. Computer Methods in Applied Mechanics and Engineering, 1988, 71 (2): 197–224.
[31] CIFUENTES A O, KALBAG A. A performance study of tetrahedral and hexahedral elements in 3-D finite element structural analysis [J]. Finite Elements in Analysis and Design, 1992, 12 (4): 313–318.
[32] GAIN A L, PAULINO G H, DUARTE L S, et al. Topology optimization using polytopes [J]. Computer Methods in Applied Mechanics and Engineering, 2015, 293: 411–430.
[33] CHI H, PEREIRA A, MENEZES I F M, et al. Virtual element method (VEM)-based topology optimization: An integrated framework [J]. Structural and Multidisciplinary Optimization, 2020, 62 (3): 1089–1113. DOI: 10.1007/s00158-019-02268-w.
[34] GIRALDOLONDOO O, PAULINO G H. PolyDyna: A Matlab implementation for topology optimization of structures subjected to dynamic loads [J]. Structural and Multidisciplinary Optimization, 2021, 63 (1): 183–205.
[35] OOMS T, VANTYGHEM G, THIENPONT T, et al. Thermoelastic topology optimization of structural components at elevated temperatures considering transient heat conduction[J]. Engineering with Computers, 2024, 40(4): 2183–2207. DOI: 10.1007/s00366-023-01907-7.